Joint reconstruction of misaligned images from incomplete measurements for cardiac MRI

Gilles Puy*, Gabriele Bonanno†‡, Matthias Stuber†‡, and Pierre Vandergheynst*
* Institute of Electrical Engineering, Ecole Polytechnique Fédérale de Lausanne (EPFL), Lausanne, Switzerland
† Department of Radiology, University Hospital (CHUV) and University of Lausanne, Lausanne, Switzerland
‡ Center for Biomedical Imaging (CIBM), Lausanne, Switzerland

***Abstract*—We present a novel method for robust reconstruction of the image of a moving object from incomplete linear measurements. We assume that only few measurements of this object can be acquired at different instants and model the correlation between measurements using global geometric transformations represented by few parameters. Then, we design a method that is able to jointly estimate these transformation parameters and an image of the object, while taking into account possible occlusions of parts of the object during the acquisitions. The reconstruction algorithm minimizes a non-convex functional and generates a sequence of estimates converging to a critical point of this functional. Finally, we show how to apply this algorithm on a real cardiac acquisition for free breathing coronary magnetic resonance imaging.**

I. Introduction

We have recently presented a method to reconstruct jointly a set of images, representing a same scene, from few linear multi-view measurements [1]. The correlation between images is modeled using global parametric transformations, such as homographies, and the proposed algorithm accurately estimates the images and the transformation parameters, while being robust to occlusions. We have shown the efficiency of the algorithm for problems such as super-resolution from multiple frames, or compressed sensing, using numerical simulations.

We show here the potential interest of this method for free breathing coronary magnetic resonance imaging (MRI) [2]. In this application, one wants to obtain a single high resolution image of the heart to visualize the coronaries. To reach this goal, one of the major challenge is to properly compensate for the respiratory motion in the image reconstruction process. Indeed, the acquisition speed in MRI is slow and inevitable motion of the heart occur during the acquisition. To suppress motion due to heart contractions, an ECG signal is usually acquired to ensure that the Fourier measurements are taken after a fixed time delay from the beginning of the cardiac cycle. A few measurements are then taken at each cycle during a period of minimum coronary motion (late diastole). Unfortunately, the number of measurements acquired during one cardiac cycle is too small to accurately reconstruct a high resolution image of the heart. One thus has to combine measurements acquired at different cycles to gather enough information. However, it is mandatory to compensate for the respiratory motion occurring between cardiac cycles to be able to visualize high resolution features.

This work was partly funded by the Hasler Foundation (project number 12080).

As shown in [3] for two-dimensional MRI of the right coronary artery, global translations are already sufficient to reach good image quality. In [3], the estimation of the transformation parameters and the image reconstruction are separated into two separate tasks. We show here that the algorithm presented in [1] can be considered as an alternative for joint registration and reconstruction.

Notations: The Euclidean scalar product of $\mathbb{R}^n$ is denoted $\langle \cdot, \cdot \rangle$ and $\| \cdot \|_2$ is the corresponding ℓ_2-norm. The ℓ_1-norm of a vector $\boldsymbol{x} = (x_i)_{1 \leqslant i \leqslant n} \in \mathbb{R}^n$ is defined as $\|\boldsymbol{x}\|_1 = \sum_{i=1}^n |x_i|$. The transpose operator is denoted $\cdot^\intercal$.

II. Joint registration and reconstruction via non-convex optimization

A. Problem formulation

Let $\boldsymbol{y}_1, \dots, \boldsymbol{y}_l \in \mathbb{R}^m$ be l independent linear observations of a moving object represented by the image $\boldsymbol{x}_0 \in \mathbb{R}^n$, $m \leqslant n$. The j^{th} vector $\boldsymbol{y}_j$ contains the measurements of the object when it is at its j^{th} position. We assume that the acquisition speed is faster than the one of the object, so that we can consider that the object is not moving during each acquisition. However, as the object is moving between two different acquisitions, the image $\boldsymbol{x}_0$ undergoes geometric transformations. In this work, we consider that these transformations are not known in advance and need to be estimated from the measurements. For simplicity, we restrict ourselves to global transformations, such as translations or homographies, that can be represented by few parameters $\boldsymbol{\theta}_j \in \mathbb{R}^q$, $j = 1, \dots, l$. We also assume that the transformed images can be well estimated using interpolation matrices $\mathsf{S}(\boldsymbol{\theta}_j) \in \mathbb{R}^{n \times n}$, $j = 1, \dots, l$, built using, e.g., bicubic splines [4]. Then, to handle more realistic acquisitions, we consider possible occlusions of the object and model them using l foreground images $\boldsymbol{x}_1, \dots, \boldsymbol{x}_l \in \mathbb{R}^n$. The image "viewed" at the j^{th} acquisition is thus $\mathsf{S}(\boldsymbol{\theta}_j)\boldsymbol{x}_0 + \boldsymbol{x}_j$. In summary, denoting by $\mathsf{A}_1, \dots, \mathsf{A}_l \in \mathbb{R}^{m \times n}$ the observation matrices, the measurement model satisfies

$$\begin{bmatrix} \boldsymbol{y}_1 \\ \vdots \\ \boldsymbol{y}_l \end{bmatrix} = \begin{bmatrix} \mathsf{A}_1\mathsf{S}(\boldsymbol{\theta}_1) & \mathsf{A}_1 & \dots & 0 \\ \vdots & \vdots & \ddots & \vdots \\ \mathsf{A}_l\mathsf{S}(\boldsymbol{\theta}_l) & 0 & \dots & \mathsf{A}_l \end{bmatrix} \begin{bmatrix} \boldsymbol{x}_0 \\ \vdots \\ \boldsymbol{x}_l \end{bmatrix} + \begin{bmatrix} \boldsymbol{n}_1 \\ \vdots \\ \boldsymbol{n}_l \end{bmatrix}, \quad (1)$$

where $\boldsymbol{n}_1, \dots, \boldsymbol{n}_l \in \mathbb{R}^m$ model additive measurement noise.

Estimating the images $\boldsymbol{x} = (\boldsymbol{x}_0^\intercal, \dots, \boldsymbol{x}_l^\intercal)^\intercal \in \mathbb{R}^{(l+1)n}$ and the transformation parameters $\boldsymbol{\theta}^\intercal = (\boldsymbol{\theta}_1^\intercal, \dots, \boldsymbol{\theta}_l^\intercal)^\intercal \in \mathbb{R}^{lq}$ using the acquired measurements $\boldsymbol{y} = (\boldsymbol{y}_1^\intercal, \dots, \boldsymbol{y}_l^\intercal)^\intercal \in \mathbb{R}^{lm}$ as sole information is an ill-posed inverse problem. Prior information is needed to restrict the set of admissible solutions. Concerning the images, we can for example search for the ones with a sparse decomposition in a wavelet basis by minimizing the ℓ_1-norm of their wavelet coefficients. Alternatively, we can search for piecewise constant images by minimizing their Total Variation norm. For the transformation parameters, we can for example impose that they belong to compact convex sets $\Theta_j = \{\boldsymbol{\theta}_j \in \mathbb{R}^q : \underline{\boldsymbol{\theta}}_j \leqslant \boldsymbol{\theta}_j \leqslant \bar{\boldsymbol{\theta}}_j\}$, $j = 1, \dots, l$, where $\underline{\boldsymbol{\theta}}_j \in \mathbb{R}^q$ and $\bar{\boldsymbol{\theta}}_j \in \mathbb{R}^q$ are pre-defined upper and lower bounds[1]. Therefore, an estimate $\boldsymbol{x}^*$ and $\boldsymbol{\theta}^*$ of the images and the transformations parameters can be obtained by solving

$$\min_{(\boldsymbol{x},\boldsymbol{\theta})} f(\boldsymbol{x}) + \kappa \, \|\mathsf{A}(\boldsymbol{\theta})\, \boldsymbol{x} - \boldsymbol{y}\|_2^2 \;\text{ subjet to }\; \boldsymbol{\theta} \in \Theta, \quad (2)$$

where $f\colon \mathbb{R}^{(l+1)n} \to \mathbb{R} \cup \{+\infty\}$ is a proper lower-semicontinuous convex function, $\kappa^{-1} > 0$ is a regularizing parameter that should be adjusted with the noise level $\|\boldsymbol{n}\|_2$, $\Theta = \{\boldsymbol{\theta} = (\boldsymbol{\theta}_1^\intercal, \dots, \boldsymbol{\theta}_l^\intercal)^\intercal \in \mathbb{R}^{lq} : \boldsymbol{\theta}_j \in \Theta_j,\ j = 1, \dots, l\}$, and

$$\mathsf{A}(\boldsymbol{\theta}) = \begin{bmatrix} \mathsf{A}_1\mathsf{S}(\boldsymbol{\theta}_1) & \mathsf{A}_1 & \dots & 0 \\ \vdots & \vdots & \ddots & \vdots \\ \mathsf{A}_l\mathsf{S}(\boldsymbol{\theta}_l) & 0 & \dots & \mathsf{A}_l \end{bmatrix} \in \mathbb{R}^{lm \times (l+1)n}.$$

Unfortunately, the minimization problem (2) is non-linear in $\boldsymbol{\theta}$ and finding a global minimizer is not trivial. Nevertheless, based on the recent works of Attouch *et al.*, [5], [6], we developed a novel minimization method for problem (2) that produces a convergent sequence to a critical point $(\boldsymbol{x}^*, \boldsymbol{\theta}^*)$ of the functional $L\colon \mathbb{R}^{(l+1)n} \times \mathbb{R}^{lq} \to \mathbb{R} \cup \{+\infty\}$ defined as

$$L(\boldsymbol{x}, \boldsymbol{\theta}) = f(\boldsymbol{x}) + \kappa \, \|\mathsf{A}(\boldsymbol{\theta})\, \boldsymbol{x} - \boldsymbol{y}\|_2^2 + i_\Theta(\boldsymbol{\theta}), \quad (3)$$

where i_Θ is the indicator function[2] of Θ. Note that $(\boldsymbol{x}^*, \boldsymbol{\theta}^*)$ is not necessarily a global minimizer of L but might only be local minimizer or a saddle point of the objective function. The proposed algorithm generates a sequence of estimates $(\boldsymbol{x}^k, \boldsymbol{\theta}^k)_{k\in\mathbb{N}}$ such that $L(\boldsymbol{x}^{k+1}, \boldsymbol{\theta}^{k+1}) \leqslant L(\boldsymbol{x}^k, \boldsymbol{\theta}^k)$, $\forall k \in \mathbb{N}$, and consists of two main steps.

B. First step of the algorithm

Let $(\boldsymbol{x}^k, \boldsymbol{\theta}^k) \in \mathbb{R}^{(l+1)n} \times \Theta$ be the estimates obtained after k iterations of the algorithm. The first step consists in finding a new estimate $\boldsymbol{x}^{k+1} \in \mathbb{R}^{(l+1)n}$ that decreases the value of the objective function L while keeping $\boldsymbol{\theta}^k$ fixed. We choose here this new estimate as a solution of

$$\min_{\boldsymbol{x}\in\mathbb{R}^{(l+1)n}} L(\boldsymbol{x}, \boldsymbol{\theta}^k) + \frac{\lambda_{\boldsymbol{x}}^k}{2}\, h_\mu(\Psi^\intercal(\boldsymbol{x} - \boldsymbol{x}^k)), \quad (4)$$

[1]Let $\bar{\boldsymbol{\theta}} = (\bar{\theta}_i)_{1\leqslant i\leqslant q} \in \mathbb{R}^q$, $\boldsymbol{\theta} = (\theta_i)_{1\leqslant i\leqslant q} \in \mathbb{R}^q$, $\boldsymbol{\theta} \leqslant \bar{\boldsymbol{\theta}}$ means that $\theta_i \leqslant \bar{\theta}_i$ for all $i \in \{1, \dots, q\}$.

[2]The indicator function of a non-empty closed convex set C is the proper lower semicontinuous convex function that satisfies $i_C(\boldsymbol{x}) = 0$ if $\boldsymbol{x} \in C$ and $i_C(\boldsymbol{x}) = +\infty$ otherwise.

where $\lambda_{\boldsymbol{x}}^k > 0$ acts as a stepsize parameter, $\Psi \in \mathbb{R}^{(l+1)n\times(l+1)p}$ is a block-diagonal matrix built by repeating $l+1$ times a wavelet tight-frame[3] $\mathsf{W} \in \mathbb{R}^{n\times p}$, $p \geqslant n$, on the diagonal, and $h_\mu\colon \mathbb{R}^{(l+1)p} \to \mathbb{R}$ is the Huber function. It is a smooth approximation of the ℓ_1-norm satisfying

$$\forall\, \boldsymbol{\alpha} = (\alpha_i)_{1\leqslant i\leqslant (l+1)p} \in \mathbb{R}^{(l+1)p}, \quad h_\mu(\boldsymbol{\alpha}) = \sum_{i=1}^{(l+1)p} h_i,$$

with

$$h_i = \begin{cases} \alpha_i^2/(2\mu), & \text{if } |\alpha_i| < \mu, \\ |\alpha_i| + \mu/2, & \text{otherwise,} \end{cases} \quad \forall i \in \{1, \dots, (l+1)p\},$$

and $\mu > 0$. In practice, the smoothing parameter μ can be chosen small so that the function h_μ behaves similarly to the ℓ_1-norm. Let us highlight that the minimization problem (4) is convex and can be solved efficiently using, e.g., the algorithm presented in [7].

We noticed experimentally that the addition of the function h_μ in the minimization procedure was improving the accuracy of the estimated signals and transformations parameters by producing a coarse-to-fine scales reconstruction of the images. This function acts as a proximal term and provides, up to some limits, a control on the evolution of the sequence of estimated images $(\boldsymbol{x}^k)_{k\geqslant 0}$. Remembering that the ℓ_1-norm favors the selection of few large coefficients, this function imposes that the next estimate $\boldsymbol{x}^{k+1}$ differs from $\boldsymbol{x}^k$ by a few large wavelet coefficients. The bigger the $\lambda_{\boldsymbol{x}}^k$ parameter is, the fewer the number of wavelet atoms that can be added at each iteration is. In practice, we start form $\boldsymbol{x}^0 = \boldsymbol{0} \in \mathbb{R}^{(l+1)n}$ and with a large value of $\lambda_{\boldsymbol{x}}^k$ at $k = 0$. We then slightly decrease the value of $\lambda_{\boldsymbol{x}}^k$ at each iteration. This allows us to have a coarse-to-fine scales reconstruction of the images, as illustrated in [1].

C. Second step of the algorithm

In the second step of the algorithm, we update the transformation parameters to further decrease the value of the objective function. As the function $\boldsymbol{\theta} \mapsto \|\mathsf{A}(\boldsymbol{\theta})\, \boldsymbol{x}^{k+1} - \boldsymbol{y}\|_2^2$ and i_Θ are separable in $\boldsymbol{\theta}_j$, $j = 1, \dots, l$, we optimize the transformation parameters separately for each observations.

To simplify the notations, we introduce l new functions $Q_j^{k+1}\colon \mathbb{R}^q \to \mathbb{R}$, with $j = 1, \dots, l$, satisfying

$$Q_j^{k+1}(\boldsymbol{\theta}_j) = \|\mathsf{A}_j\mathsf{S}(\boldsymbol{\theta}_j)\boldsymbol{x}_0^{k+1} + \mathsf{A}_j\boldsymbol{x}_j^{k+1} - \boldsymbol{y}_j\|_2^2. \quad (5)$$

One of our goal is to find parameters $\boldsymbol{\theta}_j^{k+1} \in \Theta_j$ such that $Q_j^{k+1}(\boldsymbol{\theta}_j^{k+1}) \leqslant Q_j^{k+1}(\boldsymbol{\theta}_j^k)$. These functions are non-linear in $\boldsymbol{\theta}_j$. To simplify the estimation of the parameters, we instead minimize quadratic approximations of these functions. Assuming that the entries of the matrix $\mathsf{S}(\boldsymbol{\theta}_j)$ are differentiable with respect to the transformation parameters, the first order Taylor expansion of $\mathsf{S}(\boldsymbol{\theta}_j)\boldsymbol{x}_0^{k+1}$ at $\boldsymbol{\theta}_j^k$ is $\mathsf{S}(\boldsymbol{\theta}_j^k)\boldsymbol{x}_0^{k+1} + \mathsf{J}_j^k(\boldsymbol{\theta}_j - \boldsymbol{\theta}_j^k)$ with

$$\mathsf{J}_j^k = \left(\partial_{\theta_{1j}}\mathsf{S}(\boldsymbol{\theta}_j^k)\boldsymbol{x}_0^{k+1}, \dots\ , \partial_{\theta_{qj}}\mathsf{S}(\boldsymbol{\theta}_j^k)\boldsymbol{x}_0^{k+1}\right) \in \mathbb{R}^{n\times q}.$$

[3]It satisfies $\mathsf{W}\mathsf{W}^\intercal = \mathsf{I}_n$, with $\mathsf{I}_n \in \mathbb{R}^{n\times n}$ the identity matrix.

Therefore, $Q_j^{k+1}(\boldsymbol{\theta}_j^k) + P_j^{k+1}(\boldsymbol{\theta}_j)$, with

$$P_j^{k+1}(\boldsymbol{\theta}_j) = \left\langle \nabla Q_j^{k+1}(\boldsymbol{\theta}_j^k), \boldsymbol{\theta}_j - \boldsymbol{\theta}_j^k \right\rangle + \ \|\mathsf{A}_j \mathsf{J}_j^k (\boldsymbol{\theta}_j - \boldsymbol{\theta}_j^k)\|_2^2,$$

and

$$\nabla Q_j^{k+1}(\boldsymbol{\theta}_j^k) = 2\left(\mathsf{A}_j \mathsf{J}_j^k\right)^\intercal \left(\mathsf{A}_j \mathsf{S}(\boldsymbol{\theta}_j^k)\boldsymbol{x}_0^{k+1} + \mathsf{A}_j \boldsymbol{x}_j^{k+1} - \boldsymbol{y}_j\right),$$

is a quadratic approximation of Q_j^{k+1} at $\boldsymbol{\theta}_j^k$.

To update the transformation parameters, we minimize this quadratic approximation to which we add another quadratic term that ensures a decrease of the objective function L. The next estimate of the transformation parameters is

$$\boldsymbol{\theta}_j^{k+1} = \underset{\boldsymbol{\theta}_j \in \Theta_j}{\operatorname{argmin}} \ P_j^{k+1}(\boldsymbol{\theta}_j) + \frac{2^i \lambda_{\boldsymbol{\theta}}}{2} \|\boldsymbol{\theta}_j - \boldsymbol{\theta}_j^k\|_2^2, \qquad (6)$$

where $\lambda_{\boldsymbol{\theta}} > 0$ and i is the smallest positive integer such that

$$Q_j^{k+1}(\boldsymbol{\theta}_j^{k+1}) \leqslant \ Q_j^{k+1}(\boldsymbol{\theta}_j^k) + P_j^{k+1}(\boldsymbol{\theta}_j^{k+1}) + \ \frac{(2^i - 1)\lambda_{\boldsymbol{\theta}}}{2} \|\boldsymbol{\theta}_j^{k+1} - \boldsymbol{\theta}_j^k\|_2^2. \quad (7)$$

The above condition ensures that $\boldsymbol{\theta}_j^{k+1}$ decrease the value of objective function and is essential for the convergence of the sequence $(\boldsymbol{x}^k, \boldsymbol{\theta}^k)_{k\in\mathbb{N}}$ to a critical point of L.

D. Convergence result

We are now in position to state our convergence result, whose proof can be found in [1].

Theorem 1: Let L be the objective function defined in (3) with $\kappa > 0$. Assume that L is bounded below, that the entries of S_j, with $j = 1, \ldots, l$, are twice continuously differentiable, that $\Psi \in \mathbb{R}^{(l+1)n \times (l+1)p}$ satisfies $\Psi\Psi^\intercal = \mathsf{I}_{(l+1)n}$, and that the stepsizes satisfy $0 < \underline{\lambda} \leqslant \lambda_{\boldsymbol{x}}^k, \lambda_{\boldsymbol{\theta}} \leqslant \bar{\lambda}$ for all $k \in \mathbb{N}$. Then, the sequence of estimates $(\boldsymbol{x}^k, \boldsymbol{\theta}^k)_{k\in\mathbb{N}}$ generated by the algorithm described above is correctly defined and the following statements hold:

1) For all $k \geqslant 0$,

$$L(\boldsymbol{x}^k, \boldsymbol{\theta}^k) - L(\boldsymbol{x}^{k+1}, \boldsymbol{\theta}^{k+1}) \geqslant \frac{\underline{\lambda}}{2}\left[\kappa \ \|\boldsymbol{\theta}^{k+1} - \boldsymbol{\theta}^k\|_2^2 + h_\mu(\Psi^\intercal(\boldsymbol{x}^{k+1} - \boldsymbol{x}^k))\right]. \quad (8)$$

   Hence $L(\boldsymbol{x}^k, \boldsymbol{\theta}^k)$, $k \in \mathbb{N}$, does not increase.
2) The sequences $(\boldsymbol{x}^{k+1} - \boldsymbol{x}^k)_{k\in\mathbb{N}}$ and $(\boldsymbol{\theta}^{k+1} - \boldsymbol{\theta}^k)_{k\in\mathbb{N}}$ converge. Indeed,

$$\lim_{k\to+\infty} \|\boldsymbol{x}^{k+1} - \boldsymbol{x}^k\|_2 + \|\boldsymbol{\theta}^{k+1} - \boldsymbol{\theta}^k\|_2 = 0. \qquad (9)$$

3) Assume that L has the Kurdyca-Łojasiewicz property (see Definition 3.2 in [5]). Then, if the sequence $(\boldsymbol{x}^k)_{k\in\mathbb{N}}$ is bounded, the sequence $(\boldsymbol{x}^k, \boldsymbol{\theta}^k)_{k\in\mathbb{N}}$ converges to a critical point $(\boldsymbol{x}^*, \boldsymbol{\theta}^*)$ of L.

The last point of Theorem 1 applies if L has the Kurdyca-Łojasiewicz property. As explained in [5], this property is satisfied by several classes of functions. We detail in [1] several examples where the conditions required by Theorem 1 are satisfied. For example, if the interpolation matrices S_j, $j = 1, \ldots, l$, are built using the bicubic interpolation [8] and $f(\boldsymbol{x}) = \|\Phi\boldsymbol{x}\|_1$ for some basis $\Phi \in \mathbb{R}^{(l+1)n\times(l+1)n}$, then the sequence of estimates converges to a critical point of the objective function L for geometric transformations such as translations, affine transformations or "small" homographies.

III. Free breathing coronary MRI

A. Acquisition model

We acquired 2D image data of the right coronary artery in a healthy adult subject with a clinical 3T scanner (Siemens Trio, Erlangen, Germany). The field of view was 320×320 mm and the spatial resolution was $1 \times 1 \times 8$ mm. Our goal is here to reconstruct a high resolution image $\boldsymbol{x}_0$ of the heart containing 320×320 pixels from this set of few Fourier measurements.

Note that in MRI we are dealing with complex images. For simplicity, and to be able to use the proposed algorithm without modifications, we treat separately the real and imaginary parts of the images. Therefore, the vector $\boldsymbol{x}_0$ has size $n = 2 \times 320^2$ and satisfies: $\boldsymbol{x}_0^\intercal = ((\boldsymbol{x}_0^r)^\intercal, (\boldsymbol{x}_0^i)^\intercal)$, where $\boldsymbol{x}_0^r \in \mathbb{R}^{n/2}$ and $\boldsymbol{x}_0^i \in \mathbb{R}^{n/2}$ are the real and imaginary parts of the image. The same convention is used for the foreground images. Note that the j^{th} transformed background image is now obtained by multiplication with the block-diagonal matrix built by repeating twice $\mathsf{S}(\boldsymbol{\theta}_j)$ on the diagonal. The measurements describing these images are then obtained as follows.

At each cardiac cycle, we acquire few complex Fourier coefficients lying along 15 radial lines, as presented in Fig. 1, with each line containing 320 equispaced sampling points. As before, we separate the real and imaginary parts of the measurements and stack them in a single measurement vector: $\boldsymbol{y}_j^\intercal = ((\boldsymbol{y}_j^r)^\intercal, (\boldsymbol{y}_j^i)^\intercal)$, with $\boldsymbol{y}_j^r \in \mathbb{R}^{m/2}$ and $\boldsymbol{y}_j^i \in \mathbb{R}^{m/2}$. The number of acquired measurements at each cycle satisfies $m/n = 4.7\ \%$ and a total of $l = 24$ acquisitions are performed at different cycles. Note that the radial lines along which the measurements are acquired change at each cardiac cycle to cover the Fourier space as much as possible. Let Ω_j be the set of frequencies probed at the j^{th} cycle. We model this acquisition using the complex Fourier matrix $\mathsf{F}_{\Omega_j} \in \mathbb{C}^{m/2\times n/2}$ which estimates the Fourier transform of a discrete complex image on the frequencies Ω_j. The observation matrix A_j then satisfies

$$\mathsf{A}_j = \begin{bmatrix} \mathsf{F}_{\Omega_j}^r & -\mathsf{F}_{\Omega_j}^i \\ \mathsf{F}_{\Omega_j}^i & \mathsf{F}_{\Omega_j}^r \end{bmatrix},$$

where $\mathsf{F}_{\Omega_j}^r \in \mathbb{R}^{m/2\times n/2}$ and $\mathsf{F}_{\Omega_j}^i \in \mathbb{R}^{m/2\times n/2}$ are the real and imaginary part of F_{Ω_j}.

While we are mainly interested in the reconstruction of $\boldsymbol{x}_0$, the l other foreground images have still their place in the measurement model (1). Indeed, as we are imaging one slice of an object moving in a 3D space, trough-plane motion might occur. The l foreground images can compensate for such negative effects. However, we have access to only $4.7\,\%\ n$ measurements to estimate each foreground image. We thus do not expect to obtain an accurate reconstruction of these images. On the contrary, all the $4.7\,\%\ ln$ measurements contribute to

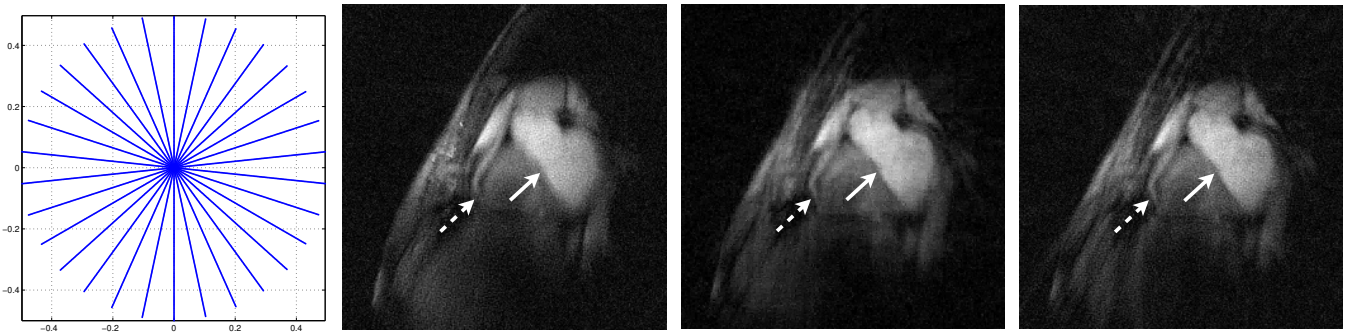

Fig. 1. From left to right: sampling pattern in Fourier space for one cardiac cycle; reconstructed image using the usual method without registration; reconstructed image $\boldsymbol{x}_0^*$ using our method; reconstructed image using the usual method with registration by the estimated parameters $\boldsymbol{\theta}^*$ obtained by our method.

the estimation of $\boldsymbol{x}_0$. Obtaining an accurate reconstruction of this reference image is thus possible.

Let us remark that we considered only one *channel* of the receiving coil in the above measurement model. In total, 32 channels are present and each of them gives access to a local image of the heart. The images of all these channels are usually combined to increase the signal-to-noise ratio of the recovered image and to have a more uniform spatial coverage. Ideally, we should also combine the measurements provided by each channel. However, the problem to solve becomes more challenging and addressing it is beyond the scope of this short abstract. We thus restrict our study to one channel only (chosen to have the best coverage of the heart).

B. Reconstruction results

We run our algorithm with $\kappa = 10^{-1}$, $\mu = 10^{-10}$, and $f(\cdot) = \|\Psi^\intercal \cdot\|_1$, where $\Psi \in \mathbb{R}^{(l+1)n \times (l+1)n}$ is built by repeating $2\,(l+1)$ times the Haar wavelet basis $\mathsf{W} \in \mathbb{R}^{n/2 \times n/2}$ on the diagonal. The transformations between cardiac cycles are assumed to be well modeled by translations. The translation parameters along both dimensions are initialised to 0 and are constrained to be in the set $[-50\,\mathrm{mm}, +50\,\mathrm{mm}]$. Finally, the stepsizes satisfy $\lambda_{\boldsymbol{x}}^k = \max((0.9)^k\, 500, 0.1)$ and $\lambda_{\boldsymbol{\theta}} = 0.1$.

Fig. 1 presents the reconstruction obtained from the acquired measurements with the proposed algorithm, as well as the ones obtained with the usual reconstruction technique *without* and *with* registration with the transformation parameters estimated by our algorithm. The usual reconstruction technique consists of a gridding operation and an inverse Fourier transform [9]. The measurements are also weighted before the gridding operation to compensate for the fact that the low frequencies are more densely sampled than the high frequencies.

Compared to the reconstruction obtained without registration, one can see that the image of the heart is sharper (see arrows) with our reconstruction method. A part the coronary previously hidden becomes visible (dotted arrow), and the borders of the blood pool and the cardiac muscle become better defined, indicating that the translations are accurately estimated. Compared to the reconstruction with registration obtained with the usual technique, our reconstruction contains less noise, though some details are slightly less visible.

IV. Conclusion

We highlighted the interest of a reconstruction technique initially developed for image reconstruction from multi-view measurements, for free breathing coronary MRI. The method reconstructs a high resolution image of the heart from few Fourier measurements and automatically compensates for the motion of the heart occurring during the acquisition. The reconstruction algorithm minimizes a non-convex functional and the generated sequence of estimates converges to a critical point of this functional.

The current technique was designed assuming that the motion can be modeled by global geometric transformations, such as translations or homographies. This is an obvious limitation of the technique which prevents us to use it with more complicated types of motion. However, the requirements of Theorem 1 hold for a large class of transformation models. This leaves us the possibility to choose more general transformations. For example, we could approximate elastic transformations using a parametric model similar to [10] and estimate the corresponding parameters using the proposed algorithm.

References

[1] Puy *et al.*, "Robust image reconstruction from multi-view measurements," *SIAM J. Imaging Sci.*, submitted, 2012. arXiv:1212.3268.

[2] Stehning *et al.*, "Free- breathing whole-heart coronary mra with 3d radial ssfp and self-navigated image reconstruction", *Magn. Reson. Med.*, vol. 54(2), pp. 476–480, 2005.

[3] Bonanno *et al.*, About the performance of multi-dimensional radial self-navigation incorporating compressed sensing for free-breathing coronary mri, *ISMRM conference*, Melbourne, 2012.

[4] Unser, "Sampling50 years after shannon," *Proc. IEEE*, vol. 88(4), pp. 569–587, 2000.

[5] Attouch *et al.*, "Proximal alternating minimization and projection methods for nonconvex problems: An approach based on the kurdyka-lojasiewicz inequality," *Math. Oper. Res.*, vol. 35(2), pp. 438–457, 2010.

[6] Attouch *et al.*, "Convergence of descent methods for semi-algebraic and tame problems: proximal algorithms, forward-backward splitting, and regularized gauss-seidel methods," *Math. Program.*, 2011.

[7] Beck *et al.*, "A fast iterative shrinkage-thresholding algorithm for linear inverse problems," *SIAM J. Imaging Sci.*, vol. 2(1), pp. 183–202, 2009.

[8] Keys, "Cubic convolution interpolation for digital image processing," *IEEE Trans. Acoustics, Speech, Signal Process.*, vol. 29(6), 1981.

[9] Jackson *et al.*, "Selection of a convolution function for fourier inversion using gridding [computerised tomography application]," *IEEE Trans. Medical Imag.*, vol. 10(3), pp. 473–478, 1991.

[10] Kybic *et al.*, "Fast parametric elastic image registration," *IEEE Trans. Image Process.*, vol. 12(11), pp. 1427–1442, 2003.